Contents lists available at ScienceDirect

Digital Chinese Medicine

journal homepage: http://www.keaipublishing.com/dcmed

Attenuation of esophageal precancerous lesions in mice by Banxia Xiexin Decoction through gut microbiota modulation

Man Jin[a†], Wenfei Zhu[a†], Zhaoling Wang[a], Kuai Yu[a], Jianping Wu[a, b], Junfeng Zhang[a*]

a. School of Medicine, Nanjing University of Chinese Medicine, Nanjing, Jiangsu 210023, China

b. Experimental Animal Center, Nanjing University of Chinese Medicine, Nanjing, Jiangsu 210023, China

ARTICLE INFO

Article history
Received 02 September 2025
Accepted 03 January 2026
Available online 25 March 2026

Keywords
Banxia Xiexin Decoction
Esophageal precancerous lesions
Gut microbiota
Transcriptome
Short-chain fatty acids

ABSTRACT

Objective To investigate the microbial mechanisms of Banxia Xiexin Decoction (半夏泻心汤, BXXXD) in the treatment of esophageal precancerous lesions.

Methods A total of 30 specific pathogen-free (SPF) grade female C57BL/6J mice were randomly assigned to a control group (n = 6) and a 4-nitroquinoline 1-oxide (4-NQO)-exposed group (n = 24). Esophageal precancerous lesions were induced by providing the 4-NQO-exposed group with 4-NQO in drinking water (100 μg/mL) for 17 consecutive weeks, whereas control group received sterile drinking water. After model establishment, the mice in 4-NQO-exposed group were further randomized into model group and three BXXXD-treated groups: low-dose (BXXXD-L, 3.7 g/kg), medium-dose (BXXXD-M, 7.4 g/kg), and high-dose (BXXXD-H, 14.8 g/kg) groups (n = 6 per group). During the subsequent intervention period, mice in control and model groups were gavaged with sterile water, while mice in BXXXD groups were gavaged once daily with the corresponding dose of BXXXD aqueous extract for 4 weeks. Histopathological changes in esophageal tissues were observed by hematoxylin and eosin (HE) staining. The fecal and esophageal microbiota were profiled via 16S rDNA high-throughput sequencing to evaluate bacterial diversity, community structure, and co-occurrence networks. BXXXD chemical fingerprints were analyzed using ultra-high-performance liquid chromatography coupled with quadrupole QExactive Orbitrap mass spectrometry (UHPLC-QE-MS). Serum short-chain fatty acids (SCFA) level was quantified by targeted metabolomics using gas chromatography-mass spectrometry (GC-MS). Transcriptomic analysis of esophageal tissues was performed to assess gene expression profiles.

Results Compared with model group, BXXXD-M group exhibited reduced mucosal hyperplasia and more orderly epithelial cell arrangement, with superior therapeutic effects in comparison with both BXXXD-L and BXXXD-H groups (P < 0.01). Microbiota analysis revealed that BXXXD increased the abundance of beneficial *Enterococcus* and reduced pathogenic *Escherichia-Shigella* in the esophagus. In the gut, BXXXD elevated the relative abundance of beneficial taxa, including *Lactobacillus*, *Dubosiella*, *Bacteroides*, and *Faecalibacterium*. Targeted metabolomics showed that BXXXD significantly reduced total serum SCFA level (P < 0.01). Transcriptomic analysis indicated that BXXXD downregulated the expression of genes associated with the progression, migration, and invasion of esophageal cancer, which were identified as kallikrein-related peptidase 6 (*Klk6*), defensin beta 4 (*Defb4*), family with

†The authors contributed equally.

*Corresponding author: Junfeng Zhang, E-mail: zhangjunfeng419@njucm.edu.cn.

Peer review under the responsibility of Hunan University of Chinese Medicine.

DOI: 10.1016/j.dcmed.2026.02.010

Citation: JIN M, ZHU WF, WANG ZL, et al. Attenuation of esophageal precancerous lesions in mice by Banxia Xiexin Decoction through gut microbiota modulation. Digital Chinese Medicine, 2026, 9(1): 114-129.

sequence similarity 3 member B (*Fam3b*), carboxypeptidase A4 (*Cpa4*), serum amyloid A1 (*Saa1*), and chitinase-like 1 (*Chil1*) ($P < 0.05$).

Conclusion BXXXD may reduce the expression levels of esophageal cancer-related genes and improve esophageal precancerous lesions through modulation of the gut microbiota and metabolites.

1 Introduction

Esophageal cancer (EC) ranks as the seventh most common malignancy worldwide, with approximately 22 100 new cases and 16 200 deaths recorded in 2025, reflecting its substantial heterogeneity [1]. EC is broadly classified into two major histological subtypes: esophageal squamous cell carcinoma (ESCC) and esophageal adenocarcinoma (EAC). In China, ESCC is the predominant form and is associated with a poorer prognosis [2]. Early-stage EC is often asymptomatic, with dysphagia being a common symptom as the disease progresses. Established risk factors include alcohol consumption, tobacco smoking, exposure to nitrosamines, gastroesophageal reflux disease (GERD), obesity, inadequate intake of fruits and vegetables, and Barrett's esophagus (BE) [3].

Emerging evidence indicates that patients with esophageal precancerous lesions who eat rapidly and prefer hot foods exhibit significant alterations in the composition of the tongue microbiota [4, 5]. Such dietary habits may influence the oral environment, including saliva secretion and the integrity of the oral mucosa, thereby shaping microbial colonization, community structure, and the homeostasis of both oral and gastrointestinal microbiota [6]. Moreover, high-fat diet-induced dysbiosis has been shown to reprogram the immune microenvironment in esophageal cancer, thereby accelerating tumor progression [7]. Conversely, modulation of the gut microbiota through probiotics or dietary interventions has demonstrated therapeutic potential in the treatment of esophageal cancer [8]. Notably, a recent study employing bidirectional Mendelian randomization (MR) analysis confirmed a bidirectional causal relationship between gut microbiota and esophageal cancer [9]. Therefore, the gut microbiota represents a promising biological target that may be exploited in the prevention and management of esophageal cancer.

Clinical studies have demonstrated that the normal esophageal microbiota is predominantly composed of members of the phyla *Firmicutes* and *Proteobacteria*, as well as the genus *Streptococcus*. In patients with EC or precancerous lesions, the relative abundance of pathogenic bacteria such as *Fusobacterium nucleatum* and *Porphyromonas gingivalis* markedly increased, whereas beneficial taxa such as *Faecalibacterium* were significantly reduced [10]. Notably, *Faecalibacterium* has been shown to induce chemotherapy resistance in ESCC by activating DNA damage pathways [11]; similarly, *Porphyromonas gingivalis* is strongly associated with ESCC [12] and promotes carcinogenesis by disrupting the mucosal barrier of the oral cavity and esophagus, facilitating the penetration of carcinogens, and activating the interleukin (IL)-6 and signal transducer and activator of transcription 3 (STAT3) signaling pathway to enhance ESCC cell proliferation and migration [13]. Taken together, these findings further support the esophageal microbiota as an important therapeutic target that may contribute to strategies for the prevention and treatment of EC.

Esophageal precancerous lesions represent a transitional stage between normal esophageal epithelium and EC. In traditional Chinese medicine (TCM), these lesions are categorized under the syndrome of dysphagia, with pathogenesis attributed to multiple factors, including spleen-stomach deficiency, upward rebellion of stomach Qi, disharmony of cold and heat, and obstruction by phlegm and blood stasis. Clinically, the therapeutic principle of "pungent to open and bitter to descend, balancing cold and heat" is frequently applied to harmonize the middle Jiao, regulate Qi, disperse nodules, and relieve symptoms, thereby contributing to the prevention and treatment of esophageal precancerous lesions. MOREIRA et al. [14] have noted significant alterations in the microbiota of both the esophagus and intestine in esophageal cancer and its precursors, suggesting that microbiota may play a critical role in the pathogenesis of EC.

Banxia Xiexin Decoction (半夏泻心汤, BXXXD) is a classical formula exemplifying this principle. Previous study has shown that BXXXD alleviates dextran sulfate sodium-induced colitis by modulating intestinal microbiota [15]. Furthermore, BXXXD has been reported to inhibit *Clostridium difficile* colonization by interfering with the binding of FadA to E-cadherin, thereby suppressing activation of the E-cadherin/β-catenin signaling pathway and delaying colitis-associated carcinogenesis [16]. Clinical study also indicates that BXXXD can mitigate chemotherapy-related toxicity in patients with advanced ESCC [17]. Taken together, these findings suggest that BXXXD may modulate the occurrence and progression of EC through regulating gut microbiota. However, the specific mechanisms underlying the effects of BXXXD on the esophageal microbiota remain unclear. Therefore, in this study, we employed a 4-nitroquinoline N-oxide (4-NQO) induced mouse models of esophageal precancerous lesions to investigate whether BXXXD improves esophageal

and intestinal microbiota as well as host metabolism. We hope that our results could provide novel evidence supporting the clinical application of BXXXD in the prevention and treatment of EC.

2 Materials and methods

2.1 Animals

A total of 30 specific pathogen-free (SPF) grade female C57BL/6J mice (weighing 13 – 15 g, 5-week-old) were purchased from Beijing Vital River Laboratory Animal Technology Co., Ltd. [Animal Experiment License No. SCXK (Jing) 2021-0006], with laboratory facility certificate No. SYXK (Su) 2018-0049. Animals were housed in the Animal Experiment Center of Nanjing University of Traditional Chinese Medicine under standard conditions: temperature maintained at 25 ± 2 °C, relative humidity at 50% – 70%, a 12-h light/dark cycle, and free access to food and water. All experimental procedures were approved by the Animal Ethics Committee of Nanjing University of Chinese Medicine (Ethics No. 202201A041).

2.2 Drugs and reagents

BXXXD was composed of Banxia (Pinelliae Rhizoma, 12 g), Huangqin (Scutellariae Radix, 9 g), Ganjiang (Zingiberis Rhizoma, 9 g), Renshen (Ginseng Radix et Rhizoma, 9 g), Zhigancao (Glycyrrhizae Radix et Rhizoma Praeparata, 9 g), Huanglian (Coptidis Rhizoma, 3 g), and Dazao (Jujubae Fructus, 4 fruits, approximately 6 g). All crude herbs were purchased from Beijing Tongrentang Nanjing Pharmacy Co., Ltd., China, and authenticated by Professor Jing Zhou, School of Pharmacy, Nanjing University of Chinese Medicine. The prescription originates from *Shanghan Lun* (《伤寒论》, *Treatise on Cold Damage Diseases)* by Zhongjing Zhang, which records the formula as: “Banxia (Pinelliae Rhizoma; washed, half a Sheng), Huangqin (Scutellariae Radix, 3 Liang), Ganjiang (Zingiberis Rhizoma, 3 Liang), Renshen (Ginseng Radix et Rhizoma, 3 Liang), Zhigancao (Glycyrrhizae Radix et Rhizoma Praeparata, 3 Liang), Huanglian (Coptidis Rhizoma, 1 Liang), and Dazao (Jujubae Fructus; split, 12 pieces)”. These dosages were converted into their modern equivalents [18]. Following established methods [19], BXXXD was prepared by decoction, after which the residues were removed. Dosages for mice were determined based on a body surface area conversion using a coefficient of 0.002 6 to convert from the human clinical equivalent dose (for a 70-kg adult) to the appropriate dose for a 20-g mouse, as guided by *Pharmacological Experimental Methods* [20]. This yielded low-, medium-, and high-dose groups of 3.7 g/kg (BXXXD-L), 7.4 g/kg (BXXXD-M), and 14.8 g/kg (BXXXD-H), corresponding to 0.5-, 1-, and 2-fold the clinical equivalent dose, respectively. The resulting decoctions were concentrated under reduced pressure to final concentrations of 0.187 5, 0.375, and 0.75 g/mL (expressed in terms of crude drug weight).

4-NQO (Dalian Meilun Biotechnology Co., Ltd., China) and 1,2-propylene glycol (analytical grade, China National Pharmaceutical Group Chemical Reagents Co., Ltd., China) were used for establishing models. 4-NQO was first dissolved in 1,2-propylene glycol to prepare a 5 mg/mL stock solution, which was stored at 4 °C in the dark. A working solution (100 μg/mL) [21] was obtained by dilution with purified water and supplied to animals in light-protected drinking bottles during model establishment.

2.3 Fingerprint analysis of BXXXD

For sample preparation, 100 mg of BXXXD extract (0.375 g/mL) was mixed with 500 μL of extraction solution, which was mixed with methanol and water in a 4 : 1 ratio. The mixture was vortexed for 30 s, homogenized at 45 Hz for 4 min, and sonicated in an ice-water bath for 1 h. After standing at – 40 °C for 1 h, the samples were centrifuged at 12 000 rpm for 15 min at 4 °C. The supernatant was filtered through a 0.22 μm microporous membrane, transferred to sample vials, and analyzed by ultra-high-performance liquid chromatography coupled with tandem mass spectrometry (UHPLC-MS/MS).

Chromatographic separation was performed on a Waters UPLC BEH C18 column (1.7 μm, 2.1 mm × 100 mm) using a UHPLC system (Vanquish, Thermo Fisher Scientific). The injection volume was 5 μL at a flow rate of 0.5 mL/min. The mobile phases consisted of 0.1% formic acid in water (A) and 0.1% formic acid in acetonitrile (B). A gradient elution was applied as follows: 85% – 25% A (0 – 11 min); 25% – 2% A (11 – 12 min); 2% A (12 – 14 min); 2% – 85% A (14 – 14.1 min); 85% A (14.1 – 16 min).

Mass spectrometry was conducted using a Q Exactive Focus system (Thermo Fisher Scientific) equipped with Xcalibur software in information dependent acquisition (IDA) mode, with a mass range between 100 and 1 500 m/z. In each acquisition cycle, the three most intense peaks were selected for UHPLC-MS/MS analysis. The parameters for the analysis were as follows: sheath gas flow, 45 Arb; auxiliary gas flow, 15 Arb; capillary temperature, 400 °C; full MS resolution, 70 000; MS/MS resolution, 17 500; normalized collision energy (NCE), 15/30/45; spray voltage, + 4.0 kV (positive mode) or – 4.0 kV (negative mode). Raw data were processed using XCMS, an R software for retention time correction, peak detection, extraction, integration, and alignment. Compound identification was performed by matching secondary MS spectra against the reference library provided by Shanghai Acuta Pharmaceuticals Co., Ltd.

2.4 Establishment of esophageal precancerous lesion mouse models and intervention by BXXXD

After being acclimatized for one week, 30 C57BL/6J mice were randomly assigned to control group (n = 6) and 4-NQO-exposed group (n = 24). The esophageal precancerous lesion mouse model was established according to a previously reported method [22]. Briefly, mice in the control group had free access to sterile drinking water, whereas mice in the 4-NQO-exposed group received 4-NQO (100 μg/mL) in drinking water ad libitum for 17 consecutive weeks. After 17 weeks, 4-NQO was discontinued and mice proceeded directly to the intervention phase without a washout period.

Mice in 4-NQO-exposed group were randomized into four subgroups (n = 6 per group): model, BXXXD-L, BXXXD-M, and BXXXD-H groups. During the 4-week intervention period, mice in the control and model groups were gavaged with sterile water, whereas mice in the BXXXD-L, BXXXD-M, and BXXXD-H groups were gavaged once daily with corresponding dose of BXXXD aqueous extract for 4 consecutive weeks.

2.5 Sample collection and processing

After intervention for 4 weeks, all mice were fasted for 24 h with free access to water. Following anesthesia induced by intraperitoneal injection of 1% pentobarbital sodium (0.2 mL/kg), blood samples were collected, after which the mice were euthanized by cervical dislocation. Subsequently, the animals were instantly dissected under sterile conditions to isolate their esophagus and collect fecal samples. Blood samples were clotted at room temperature for 30 min and centrifuged at 3 000 rpm for 10 min at 4 °C. The serum was immediately snap-frozen in liquid nitrogen and stored at – 80 °C for targeted metabolomics analysis of short-chain fatty acids (SCFA). The esophagus was rinsed with physiological saline, fixed in 4% neutral paraformaldehyde, embedded in paraffin, sectioned, and stained with hematoxylin and eosin (HE) for histopathological evaluation. Fecal samples were snap-frozen in liquid nitrogen and stored at – 80 °C for subsequent analysis of gut microbiota.

2.6 Gut microbiota sequencing and analysis

Fecal samples and esophageal contents were collected under sterile conditions. Microbial DNA was extracted from both sample types according to established methods [23]. After quality assessment, the V3 – V4 variable region of the 16S rRNA gene was amplified with the primers 341F (5′-CCTAYGGGRBGCASCAG-3′) and 806R (5′-GGACTACNNGGGTATCTAAT-3′). The amplified products were quantified using the QuantiFluor™-ST Blue Fluorescent Quantification System (Promega Corporation). A paired-end library (Illumina PE250) was constructed, and sequencing was performed by Shanghai Ling'en Biotechnology Co., Ltd. Raw sequencing reads underwent quality filtering, after which high-quality sequences were assembled and clustered into operational taxonomic units (OTUs) at 97% consistency. Bioinformatics analyses were carried out using Visual Genomics software (Release 1, Shanghai Yingfei Biotechnology Co., Ltd., China). These included microbial community structure analysis, linear discriminant analysis (LDA), and functional prediction of microbial communities using Phylogenetic Investigation of Communities by Reconstruction of Unobserved States (PICRUSt) based on Kyoto Encyclopedia of Genes and Genomes (KEGG) pathways. Community structure was visualized using Origin 2022 (OriginLab Corporation), while LDA and PICRUSt-predicted functions were visualized using Hiplot Pro (https://hiplot.com.cn/).

2.7 Targeted metabolomics analysis of SCFA

To investigate alterations in SCFA profiles among different groups, targeted metabolomics analysis of SCFAs was performed using gas chromatography-mass spectrometry (GC-MS). After thawing, 0.1 mL of serum was transferred into a 1.5 mL Eppendorf (EP) tube, followed by the addition of 0.05 mL of 50% H_2SO_4 and 0.2 mL of extraction solution (methyl tert-butyl ether containing 25 mg/L of 2-methylpentanoic acid as an internal standard). The mixture was vortexed for 10 s, shaken for 10 min, and then sonicated in an ice-water bath for 10 min. The samples were centrifuged at 10 000 rpm for 15 min at 4 °C and placed at – 20 °C for 30 min. Finally, the supernatant was collected and transferred into sample vials for GC-MS analysis.

GC-MS was performed using a GC2030-QP2020 NX system (Shimadzu, Japan) equipped with an Agilent HP-FFAP capillary column (30 m × 250 μm × 0.25 μm, J&W Scientific, USA). A 1 μL sample was injected in a 5 : 1 split mode. Helium served as the carrier gas with a septum purge flow rate of 3 mL/min and a constant column flow of 1 mL/min. The temperature program was set as follows: initial temperature at 80 °C for 1 min, increased at 10 °C/min to 200 °C and held for 5 min, then increased at 40 °C/min to 240 °C and held for 1 min. The injector, transfer line, quadrupole, and ion source temperatures were set at 240, 240, 150, and 200 °C, respectively. Electron ionization was conducted at – 70 eV with a 3.5 min solvent delay. Mass spectra were acquired in full scan mode over an m/z range of 33 – 150. Data were analyzed by matching chromatographic peaks against a reference database of 11 SCFA standards (including acetic acid, propionic acid, and butyric acid). 2-Methylpentanoic acid was used as an internal standard to quantify SCFA concentrations.

2.8 Transcriptomic analysis and reverse transcription-quantitative polymerase chain reaction (RT-qPCR) of esophageal tissue

2.8.1 RNA sequencing and differential gene expression analysis Total RNA was extracted from mouse esophageal tissue using the TRIzol® reagent kit, following a previously described protocol [24]. RNA concentration and integrity were evaluated by 1.2% agarose gel electrophoresis. mRNA was reversely transcribed into cDNA, which was subsequently end-repaired and used for cDNA library construction. The library was amplified by bridge PCR and sequenced on an Illumina NovaSeq 6000 platform. Raw sequencing reads were subjected to quality control using Trimmomatic, and the resulting clean reads were aligned to the reference genome with TopHat. Transcriptome assembly was performed with Cufflinks. Gene expression levels were quantified based on the number of reads mapped to genomic regions. Differential expression analysis was conducted using edgeR, with differentially expressed genes (DEGs) identified using the thresholds of a false discovery rate (FDR) $\leqslant 0.05$ and $|\log_2$ fold change (FC)$| \geqslant 1$. KEGG pathway enrichment analysis of the DEGs was performed using KEGG Orthology Based Annotation System (KOBAS).

2.8.2 Validation by RT-qPCR Total RNA was extracted using TRIzol extraction reagent (Aikori Biotechnology Co., Ltd., China). The RNA was then reverse transcribed into cDNA using RT MasterMix (CWBIO, China), and quantitative PCR was performed using SuperStar Universal SYBR Master Mix (CW3360M; CWBIO, China). The relative mRNA levels were calculated by the $2^{-\Delta\Delta Ct}$ method, with normalization to β-actin (*Actb*) as the internal control. The specific forward and reverse primers employed for the target genes are listed in Table 1.

Table 1 The oligonucleotide sequences of primers used for RT-qPCR

Gene symbol	Forward primer (5′-3′)	Reverse primer (5′-3′)
Klk6	CCTACCCTGGCAAGATCAC	GGATCCATCTGATATGAGTGC
Defb4	CTCCACTTGCAGCCTTTACC	GTGCATCCCCTAGAACTGGA
Fam3b	GCGACAAGTATGCCAAGA	GACGACAGCAATGTTTATCC
Cpa4	CAGCTGCTGATGTATCCCTATG	TACTTAGTGCCCGAGAGAGAA
Saa1	ACATGAAGGAAGCTGGCTGGAA	ATGTCTGTTGGCTTCCTGGTCA
Chil1	ACGATTTCCATGGAGTCTGG	AATCCTTCCCCTGAGATTGG
Actb	GGCTGTATTCCCCTCCATCG	CCAGTTGGTAACAATGCCATGT

Klk6, kallikrein-related peptidase 6. *Defb4*, defensin beta 4. *Fam3b*, family with sequence similarity 3 member B. *Cpa4*, carboxypeptidase A4. *Saa1*, serum amyloid A1. *Chil1*, chitinase-like 1.

2.9 Statistical analysis

All statistical analyses were performed using SPSS 26.0, and graphs were generated using GraphPad Prism 9.0. Data were tested for normality prior to analysis. For normally distributed data, one-way analysis of variance (ANOVA) was used; for non-normally distributed data, the nonparametric Kruskal-Wallis test was applied. Spearman's correlation analysis was conducted to assess relationships between the relative abundance of gut microbial genera and SCFA levels in control, model, and BXXXD-M groups. In addition, Spearman's correlation coefficients were calculated between esophageal and intestinal microbial genera to construct co-occurrence networks. Only correlations exceeding a predefined $|r|$ threshold with $P < 0.05$ were retained for network construction and visualization. All tests were two-tailed, and $P < 0.05$ was considered statistically significant.

3 Results

3.1 Chemical fingerprint analysis of BXXXD

Using ultra-high-performance liquid chromatography coupled with quadrupole QExactive Orbitrap mass spectrometry (UHPLC-QE-MS) analysis, a total of 314 peaks were detected in positive ion mode (Figure 1A) and 149 peaks in negative ion mode of BXXXD sample

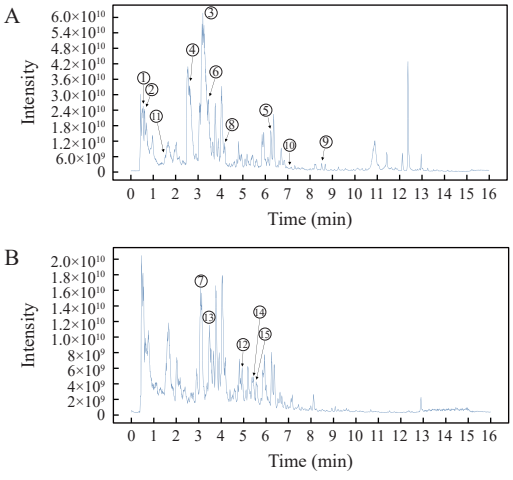

Figure 1 Chemical fingerprint analysis of BXXXD by UHPLC-QE-MS

A, total ion chromatogram (TIC) in positive ion mode. B, TIC in negative ion mode. The numbered labels indicate peak numbers of representative major constituents with peak assignments, and the compound identification details are provided in Table 2.

(Figure 1B). Representative compounds identified in the decoction included adenosine, berberine hydrochloride, scutellarin (skullcapflavone II), 6-shogaol, isolicoflavonol, and ginsenoside Rg1 (Table 2).

Table 2 Representative major compounds of BXXXD identified in the ion chromatogram

Label	Compound	Source herb	Retention time (min)	Intensity (a.u.)
①	Arginine	Banxia (Pinelliae Rhizoma)	0.51	17 979 802 250
②	Adenosine	Banxia (Pinelliae Rhizoma)	0.61	734 343 886
③	Berberine hydrochloride	Huanglian (Coptidis Rhizoma)	3.21	67 946 757 028
④	Epiberberine	Huanglian (Coptidis Rhizoma)	2.59	27 658 811 346
⑤	Skullcapflavone Ⅱ	Huangqin (Scutellariae Radix)	6.24	8 540 086 609
⑥	Wogonin	Huangqin (Scutellariae Radix)	3.57	2 774 562 990
⑦	Baicalein	Huangqin (Scutellariae Radix)	3.11	1 500 009 718
⑧	Gingerenone A	Ganjiang (Zingiberis Rhizoma)	4.2	443 068 660
⑨	6-Shogaol	Ganjiang (Zingiberis Rhizoma)	8.52	365 486 824
⑩	Isolicoflavonol	Zhigancao (Glycyrrhizae Radix et Rhizoma Praeparata)	7.14	398 556 508
⑪	Neoliquiritin	Zhigancao (Glycyrrhizae Radix et Rhizoma Praeparata)	1.56	327 928 321
⑫	Licoricesaponin G2	Zhigancao (Glycyrrhizae Radix et Rhizoma Praeparata)	4.93	1 493 417 079
⑬	Ginsenoside Rg1	Renshen (Ginseng Radix et Rhizoma)	3.46	969 293 662
⑭	Ginsenoside Ro	Renshen (Ginseng Radix et Rhizoma)	5.41	324 509 823
⑮	Ginsenoside Rf	Renshen (Ginseng Radix et Rhizoma)	4.88	121 007 288

3.2 Ameliorative effects of BXXXD on 4-NQO-induced esophageal precancerous lesions

Mouse models with 4-NQO-induced esophageal precancerous lesions were used to evaluate the therapeutic efficacy of BXXXD following a 4-week treatment period. In the control group, the esophagus appeared smooth, slender, and uniform in thickness along its entire length. In contrast, the esophagus of mice in model group exhibited marked pathological changes, including shortened and thickened esophagus, pronounced thickness in the middle and lower segments, and irregular surface protrusions. Following BXXXD administration, differential effects across doses were observed. In BXXXD-L group, the esophagus remained thickened with numerous irregular protrusions. BXXXD-M group showed a marked reduction in esophageal thickening compared with both model and BXXXD-H groups, presenting more uniform thickness, smoother surface, and fewer irregular protrusions. In BXXXD-H group, esophageal thickening was less severe than that in model group, although surface protrusions remained relatively prominent. These macroscopic observations suggested that BXXXD-M exerted the most significant therapeutic effects on esophageal precancerous lesions (Figure 2A). These findings were supported by HE staining of esophageal sections (Figure 2B). Consistently, inflammation scores were markedly elevated in the model group, whereas BXXXD treatment reduced these scores, with the BXXXD-M group showing the lowest inflammation score and the most prominent improvement (Figure 2C, $P < 0.05$, $P < 0.01$, or $P < 0.001$). HE staining revealed that the control group exhibited an intact basement membrane, uniformly thin epithelium, and orderly cell arrangement. In contrast, the model group displayed disrupted mucosal architecture, increased thickness in epithelium, the presence of atypical cells, and dysplasia, confirming the successful induction of esophageal precancerous lesions by 4-NQO. Compared with model group, BXXXD-M group showed reduced epithelial proliferation, more organized cellular arrangement, and significantly attenuated lesion severity. However, both BXXXD-L and BXXXD-H groups continued to exhibit pronounced mucosal hyperplasia, disordered cellular architecture, and a larger number of atypical cells. These results indicated that the administration of BXXXD-M effectively ameliorated 4-NQO-induced

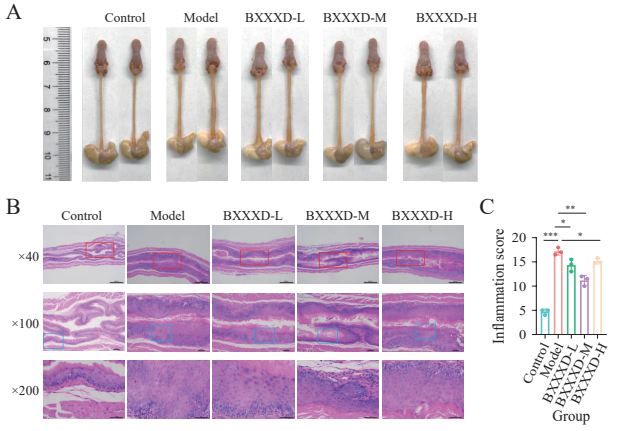

Figure 2 Therapeutic effects of BXXXD on 4-NQO-induced esophageal precancerous lesions in mice

A, gross morphological changes of the esophagus following a 4-week BXXXD treatment. B, histopathological analysis of esophageal precancerous lesions by HE staining. C, quantitative analysis of inflammation scores in esophageal tissues. $^{*}P < 0.05$, $^{**}P < 0.01$, and $^{***}P < 0.001$.

esophageal precancerous lesions in mice. Based on the macroscopic and histopathological results showing that BXXXD-M produced the greatest improvement, we selected control, model, and BXXXD-M groups for subsequent multi-omics analyses to interrogate the mechanisms underlying the most effective intervention.

3.3 Effects of BXXXD on the esophageal microbiota in mice with esophageal precancerous lesions

Analysis of α diversity in the esophageal microbiota revealed no significant differences among control, model, and BXXXD-M groups ($P > 0.05$) (Figure 3A – 3E). Similarly, β diversity analysis showed that the microbial communities from these groups did not form distinct clusters in the two-dimensional (2D) ordination space (Figure 3F). At the phylum level, the dominant taxa found in the esophagus of mouse models were Firmicutes (42.5%), Proteobacteria (36.7%), Bacteroidota (13.2%), and Actinobacteriota (6.9%) (Figure 3G). At the genus level, dominant bacteria (relative abundance > 2%) included *Ligilactobacillus* (41.0%), *Vibrionimonas* (9.7%), *Bradyrhizobium* (7.0%), *Mycobacterium* (6.7%), *Mesorhizobium* (4.3%), *Escherichia-Shigella* (4.2%), *Methylobacterium-Methylorubrum* (3.6%), *Methylovirgula* (2.5%), and *Pseudolabrys* (2.1%) (Figure 3H). LDA further demonstrated that Erysipelotrichaceae was enriched in control group, whereas Gemmatimonadota, Cyanobacteria, Blastocatellia, *Cyanobacteriia*, and Rickettsiales were enriched in model group. In contrast, *Escherichia-Shigella*, *Staphylococcus*, and *Enterococcus* were enriched in BXXXD-M group (Figure 3I). These findings suggested that BXXXD treatment modulated the esophageal microbiota by promoting the relative abundance of *Enterococcus,* which may represent a potentially beneficial shift in the microbial community.

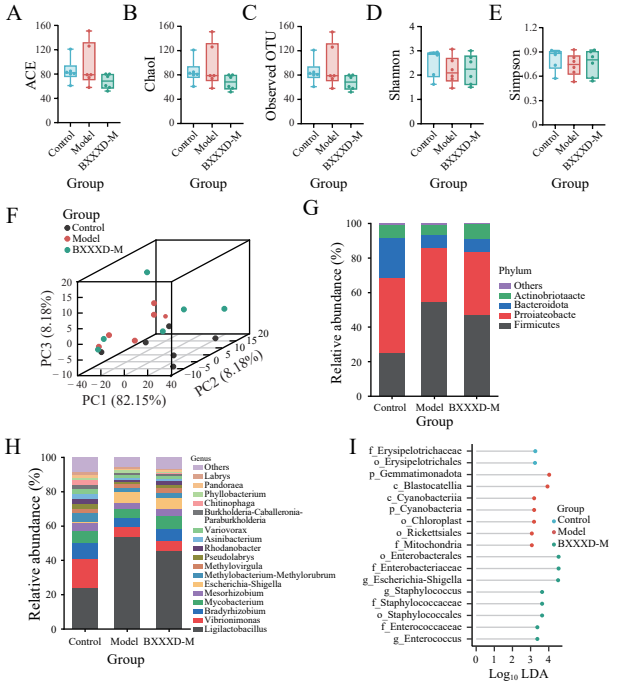

Figure 3 Analysis of the esophageal microbiota in mice with esophageal precancerous lesions treated with BXXXD

A – E, α diversity indices of the esophageal microbiota [abundance-based coverage estimator (ACE), Chao1, observed OTUs, Shannon, and Simpson, respectively]. F, β diversity of the esophageal microbiota. G, community composition at the phylum level. H, community composition at the genus level. I, LDA of differential taxa associated with BXXXD-M treatment.

3.4 Modulation of the gut microbiota by BXXXD in mice with esophageal precancerous lesions

Analysis of the gut microbiota revealed that the dominant phyla in the intestines were Firmicutes (57.4%), Bacteroidetes (38.2%), Actinobacteria (2.6%), Verrucomicrobia (0.9%), and Proteobacteria (0.7%) (Figure 4A). At the genus level, the dominant taxa (relative abundance > 1%) included *Lactobacillus*, *Helicobacter*, and others (Figure 4B).

LDA analysis demonstrated that beneficial bacteria such as *Lactobacillus*, *Dubosiella*, *Bifidobacterium*, and *Limosilactobacillus* were enriched in control group. In contrast, taxa including *Prevotellaceae UCG-001*, *Ruminococcus*, *Oscillibacter*, and *Escherichia-Shigella* were enriched in the model group, whereas *Bacteroides*, *Collinsella*, *Faecalibacterium*, and the *Eubacterium hallii* group were enriched in BXXXD-M group (Figure 4C). Functional prediction by PICRUSt further indicated that pathways such as aminoacyl-tRNA biosynthesis, mismatch repair, and glycerophosphate metabolism were enriched in control group. In model group, fatty acid biosynthesis and cysteine-methionine metabolism were predominant, while glycine, serine, and threonine metabolism, sulfur metabolism, and ascorbate and aldarate metabolism were enriched in BXXXD-M group (Figure 4D). Collectively, these findings suggested that BXXXD treatment significantly reshaped the gut microbiota in mice with esophageal precancerous lesions and enhanced functional pathways associated with amino acid metabolism.

3.5 Effects of BXXXD on SCFA in mice with esophageal precancerous lesions

Analysis of targeted metabolomics showed that total SCFA level tended to be higher in model group than that in control group, without reaching statistical significance ($P > 0.05$). In contrast, total SCFA level in BXXXD-M group was significantly lower than those in model and control groups ($P < 0.05$). Acetic acid was the predominant SCFA, accounting for approximately 70% of total SCFA. Its level was significantly elevated in model group compared with control group ($P < 0.05$) and was markedly reduced in BXXXD-M group compared with model

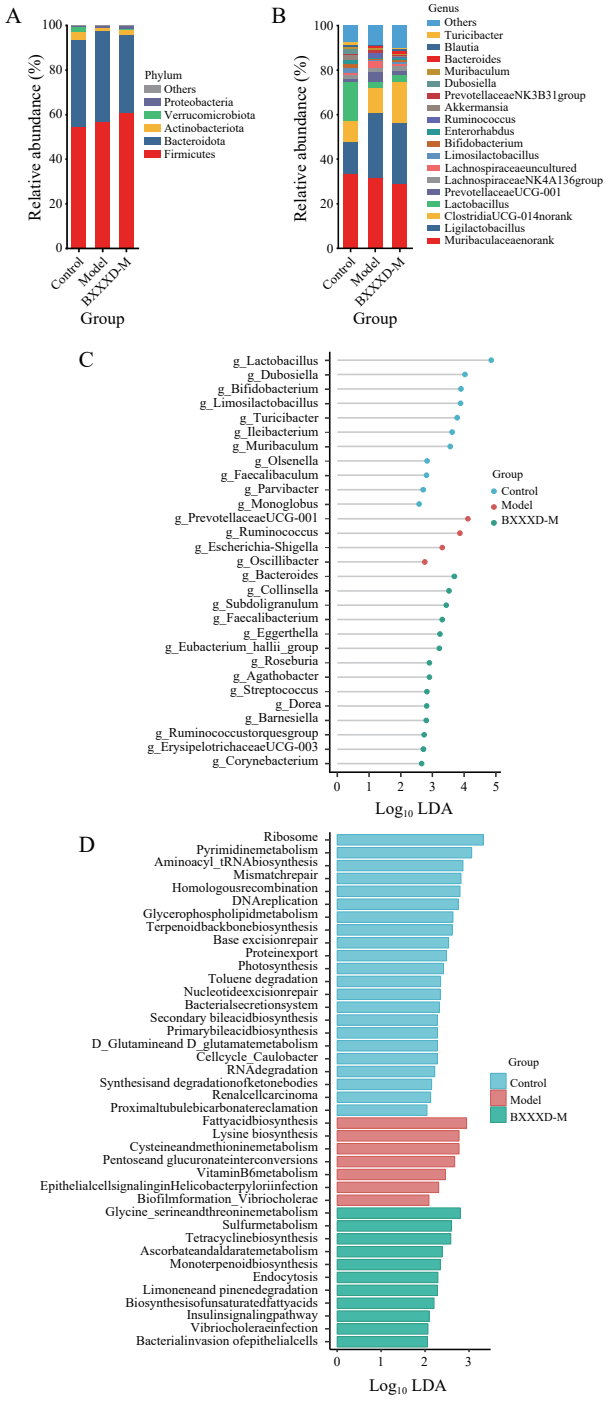

Figure 4 Analysis of the intestinal microbiota in mice with esophageal precancerous lesions treated with BXXXD

A, gut microbial community composition at the phylum level. B, gut microbial community composition at the genus level. C, LDA of differential genera associated with BXXXD-M treatment. D, PICRUSt-based functional prediction of gut microbiota associated with BXXXD treatment.

group ($P < 0.01$). For other SCFA, no significant differences were observed between model and BXXXD-M groups ($P > 0.05$). Although isobutyric acid, isovaleric acid, and valeric acid were lower in both the model group and BXXXD-M group compared with control group, and decanoic acid was higher in model group than that in control group. Collectively, these results indicate that BXXXD-M primarily reduced total SCFA and acetic acid, whereas most individual SCFA showed no significant differences between model and BXXXD-M groups (Figure 5).

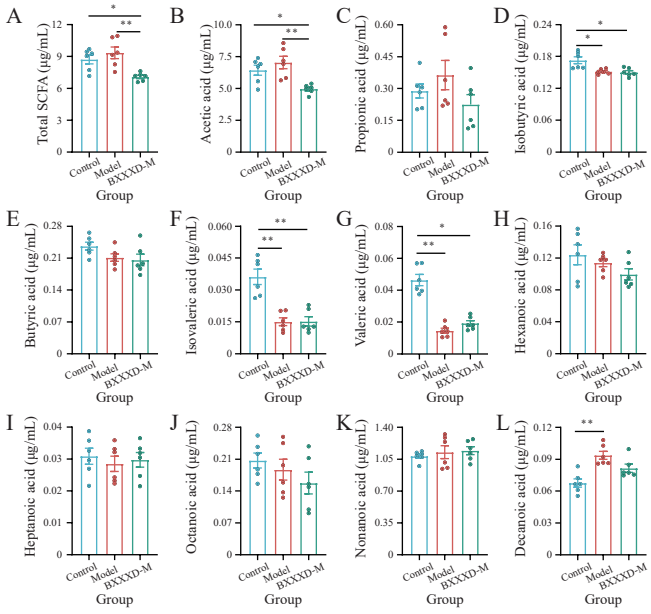

Figure 5 Targeted metabolomic analysis of serum short-chain fatty acids in mice with esophageal precancerous lesions treated with BXXXD

A, total SCFA. B, acetic acid. C, propionic acid. D, isobutyric acid. E, butyric acid. F, isovaleric acid. G, valeric acid. H, hexanoic acid. I, heptanoic acid. J, octanoic acid. K, nonanoic acid. L, decanoic acid. $^{*}P < 0.05$ and $^{**}P < 0.01$.

3.6 Correlation analysis between differential gut bacterial genera and SCFA

Spearman's correlation analysis was performed to explore potential relationships between differentially abundant gut bacterial genera and SCFA. It was found that acetate was positively correlated with *Prevotellaceae UCG-001*, *Ruminococcus*, *Muribaculum*, *Faecalibaculum*, and *Dubosiella* ($P < 0.05$), but was significantly negatively correlated with the *Ruminococcus torques* group ($P < 0.01$). Decanoate exhibited a significant positive correlation with *Ruminococcus* and *Oscillibacter* ($P < 0.05$), while showing negative correlations with beneficial genera such as *Limosilactobacillus*, *Lactobacillus*, and *Bifidobacterium* ($P < 0.05$). Isobutyric acid, valeric acid, and isovaleric acid clustered together, displaying positive correlations with *Limosilactobacillus*, *Lactobacillus*, *Bifidobacterium*, and *Dubosiella* ($P < 0.01$), which were enriched in the control group. In contrast, SCFA showed negative correlations with *Prevotellaceae UCG-001*, *Bacteroides*, *Escherichia-Shigella*, and *Corynebacterium* ($P < 0.05$) (Figure 6). Together, these findings indicated that gut microbial composition was significantly associated with SCFA profiles, suggesting a close interplay between the gut microbiota and host metabolism.

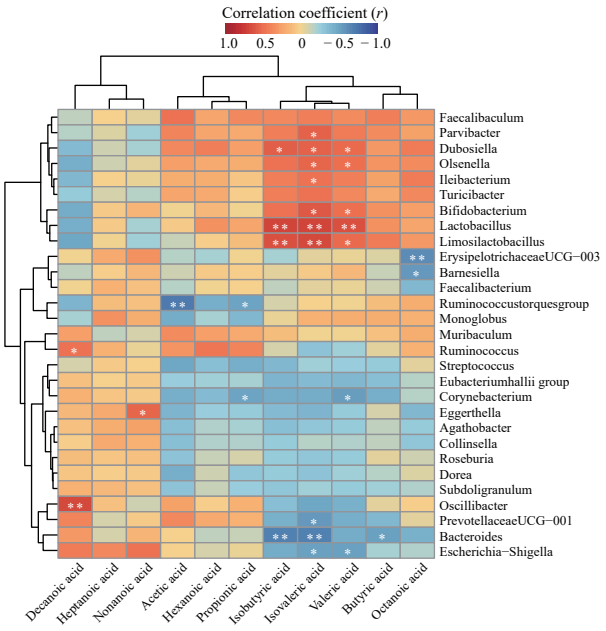

Figure 6 Correlation between differential gut bacterial genera and serum SCFA in mice

$^{*}P < 0.05$ and $^{**}P < 0.01$.

3.7 Effects of BXXXD on the genetic expression profile of esophageal precancerous lesions in mice

Principal component analysis of esophageal transcriptomes revealed distinct intra-group clustering. The control and BXXXD-M groups were closely clustered in spatial distribution, whereas model group was clearly separated (Figure 7A). DEGs were identified using thresholds of $|\log_2 FC| \geqslant 1$ and FDR < 0.05. Compared with control group, model group exhibited 512 significantly upregulated genes and 130 markedly downregulated genes (Figure 7B). Compared with model group, BXXXD-M group exhibited 182 significantly upregulated and 77 downregulated genes (Figure 7C). KEGG pathway enrichment analysis indicated that model group was enriched in pathways related to oxidative stress regulation (e.g., glutathione metabolism) and inflammation, including the tumor necrosis factor (TNF), nucleotide-binding oligomerization domain (NOD)-like receptor, and IL-17 signaling pathways (Figure 7D). Meanwhile, BXXXD-M group was enriched in pathways associated with cell cycle regulation, chemokine, peroxisome proliferator-activated receptor (PPAR), and the IL-17 signaling pathways (Figure 7E). Notably, the IL-17 signaling pathway appeared in both enrichment analyses (Figures 7D and 7E), suggesting that IL-17-related genes are involved in both lesion development and the response to BXXXD-M treatment. Venn analysis of DEGs identified 99 overlapping genes. Among them, inflammation- and stress-related genes such as *Klk6*, *Defb4*, *Fam3b*, *Cpa4*, *Saa1*, and *Chil1* were markedly upregulated in model group. BXXXD-M treatment reversed these changes, restoring their expression levels comparable to those in control group ($P > 0.05$) (Figure 7F). To further validate the RNA-seq data, RT-qPCR analysis was performed on the six DEGs. Model group exhibited significantly higher expression levels of *Klk6*, *Defb4*, *Fam3b*, *Cpa4*, *Saa1*, and *Chil1* than control group ($P < 0.05$ or $P < 0.01$). BXXXD-M treatment significantly attenuated these increases compared with model group ($P < 0.05$ or $P < 0.01$), partially reversing the expression changes toward control levels (Figure 7G – 7L). These results suggested that BXXXD-M exerted therapeutic effects on esophageal precancerous lesions by suppressing the expression of inflammation-related genes and modulating key signaling pathways.

3.8 Co-occurrence network analysis of the esophageal and intestinal microbiota in mice

The esophagus and intestine represent distinct ecological niches within the digestive tract. Previous study has suggested that disease onset can influence microbial exchange between the oral cavity and the intestine [25]. To investigate potential interactions between these niches, Spearman's correlation analysis was performed on the top 30 most abundant genera from the esophageal and intestinal microbiota in mice, with co-occurrence networks constructed. In control group, the dominant intestinal family-level taxon Lachnospiraceae_unclassified was positively correlated with the dominant esophageal genera *Methylobacterium-Methylorubrum*, *Pajaroellobacter*, *Pandoraea*, *Variovorax*, *Rhodopseudomonas*, and *Hyphomicrobium*, but negatively correlated with *Meiothermus* and *Methylovirgula*. In the model group, the dominant intestinal genus *Parabacteroides* was positively correlated with esophageal genera including *Methylobacterium-Methylorubrum*, *Labrys*, *Variovorax*, *Pseudolabrys*, *Asinibacterium*, *Rhodopseudomonas*, *Pandoraea*, *Pajaroellobacter*, and *Hyphomicrobium*, while showing a negative correlation with *Meiothermus*. In BXXXD-M group, the dominant intestinal genus *Ligilactobacillus* was negatively correlated with esophageal genera such as *Hyphomicrobium*, *Pajaroellobacter*, *Pandoraea*, *Asinibacterium*, *Phyllobacterium*, *Rhodopseudomonas*, and *Variovorax*. Conversely, esophageal *Ligilactobacillus* showed positive correlations with intestinal *Alistipes* and Muribaculaceae_norank, but a negative correlation with the Lachnospiraceae NK4A136 group (Figure 8).

Further analysis revealed distinct shifts in these microbial associations. Compared with control group, intestinal Parabacteroides in model group displayed strong positive correlations with the esophageal genera such as *Pajaroellobacter*, *Pandoraea*, and *Hyphomicrobium*, and a negative correlation with *Meiothermus*. In comparison

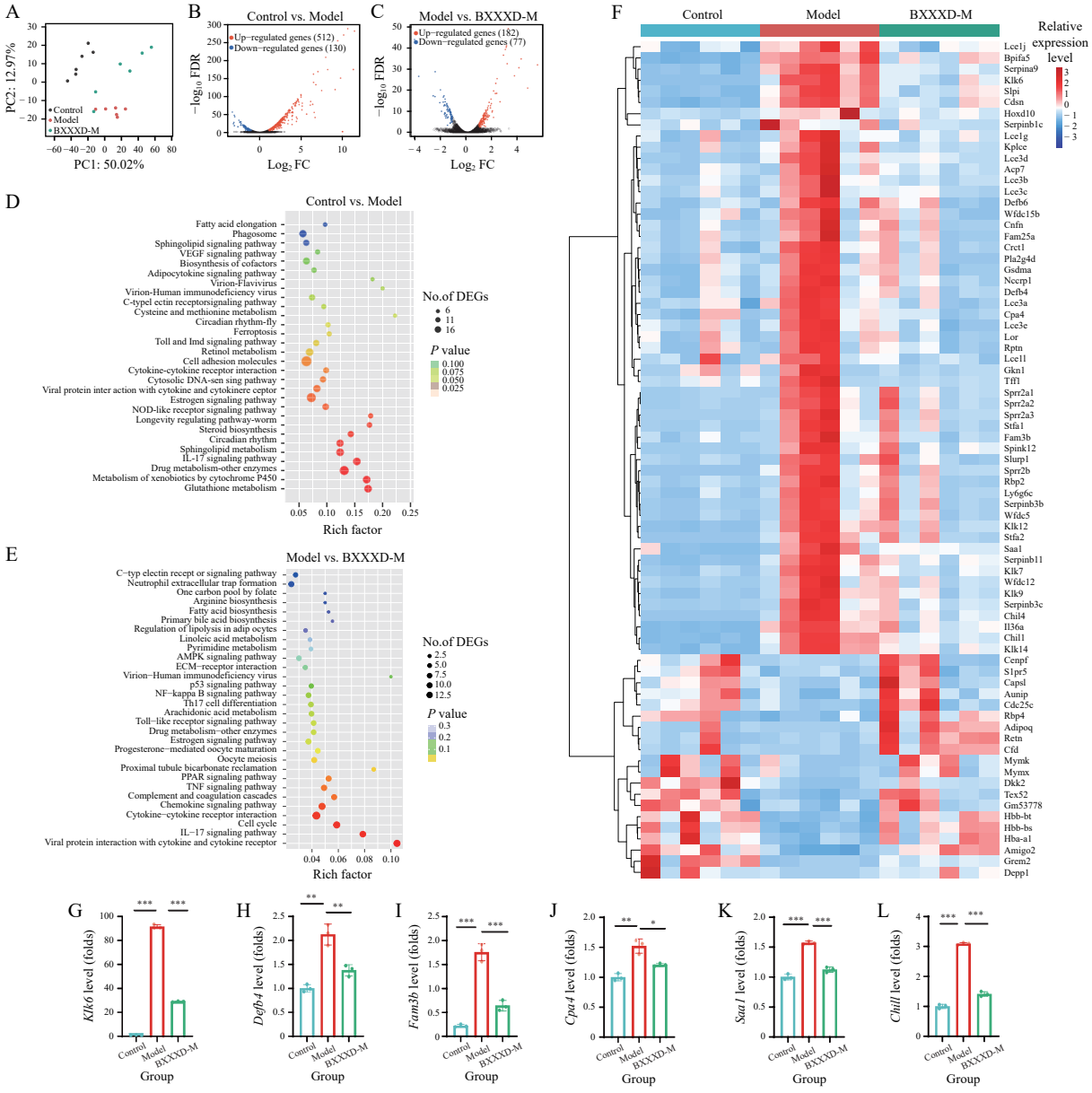

Figure 7 Effects of BXXXD on genetic expression profile of esophageal precancerous lesions in mice

A, principal component analysis of transcriptome profiles. B, DEGs between control and model groups. C, DEGs between model and BXXXD-M groups. D, KEGG pathway enrichment analysis of DEGs between control and model groups. E, KEGG pathway enrichment analysis of DEGs between model and BXXXD-M groups. F, hierarchical clustering analysis of DEGs following BXXXD treatment. G – L, relative mRNA expression levels of *Klk6*, *Defb4*, *Fam3b*, *Cpa4*, *Saa1*, and *Chil1* in mouse esophageal tissue, respectively. $^{*}P < 0.05$, $^{**}P < 0.01$, and $^{***}P < 0.001$.

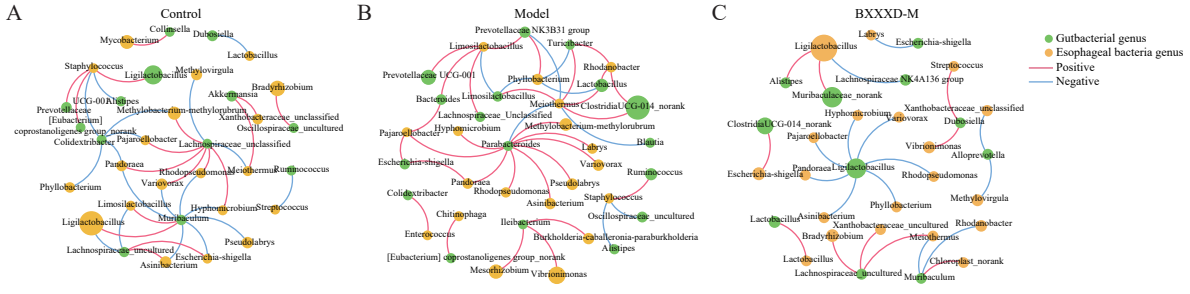

Figure 8 Co-occurrence networks between dominant bacterial genera in the esophagus and intestine

A, control group. B, model group. C, BXXXD-M group. Panels A – C show the co-occurrence patterns among the top 30 genera in each niche (esophagus and intestine) for the corresponding group. Node sizes corresponds to genus abundance, with yellow nodes representing dominant genera in the esophagus, and green nodes representing dominant genera in the intestine. Edges indicate significant correlations ($P < 0.05$), with red lines indicating positive correlations and blue lines indicating negative correlations.

to model group, BXXXD-M group showed positive correlations between intestinal Muribaculaceae_norank and esophageal *Ligilactobacillus*, and negative correlations between intestinal Lachnospiraceae and esophageal *Ligilactobacillus*.

Overall, BXXXD treatment disrupted the pathogenic synergy observed in model group by dissociating the positive correlations between intestinal *Parabacteroides* and esophageal pathogenic genera such as *Pandoraea*. This intervention reversed the antagonistic relationships with protective taxa like *Meiothermus*, partially restoring the microbial interaction network to a state resembling that of control group.

4 Discussion

4.1 BXXXD-mediated amelioration of 4-NQO-induced esophageal precancerous lesions

An imbalance in the microbiota is increasingly recognized as a potential driver in the development of gastrointestinal tumors, including colorectal cancer [26]. In this study, we demonstrated that BXXXD-M significantly ameliorated 4-NQO-induced esophageal precancerous lesions in mice. Both macroscopic observation and histopathological evaluation revealed that BXXXD-M group exhibited more pronounced improvements in esophageal structure and epithelial organization than BXXXD-L and BXXXD-H groups. Collectively, these results support a non-monotonic dose-response pattern, with the medium dose achieving optimal therapeutic efficacy. The lack of further benefit at the high dose may reflect saturation of key targets, increased gastrointestinal burden, or overcorrection of the microbial ecosystem at excessive dosing, which could partially offset therapeutic benefits. Further studies are needed to clarify these mechanisms.

4.2 Remodeling of esophageal microbiota composition by BXXXD via modulation of key taxa

Analysis of esophageal microbiota revealed distinct microbial signatures associated with each experimental group: Erysipelotrichaceae was enriched in control group, Gemmatimonadota in model group, and *Enterococcus* in BXXXD-M group. Erysipelotrichaceae, commonly found in the gastrointestinal tract of healthy individuals, contributes to mucosal barrier integrity and energy metabolism [27]. Its depletion in model group suggests compromised esophageal barrier function. Conversely, Gemmatimonadota, often isolated from soil, is regarded as an indicator of ecological stress or disruption [28]. Its enrichment in model group suggests mucosal barrier dysfunction and local microecological disturbance, which may facilitate colonization by exogenous bacteria.

Notably, although α and β diversity indices did not differ significantly among groups, this did not diminish the biological importance of the observed microbial alterations. Increasing evidence suggests that disease-associated dysbiosis is often driven by compositional shifts in specific taxa rather than global changes in diversity. In the present study, BXXXD markedly reshaped key esophageal microbial taxa even as overall diversity metrics remained stable, highlighting that microbial composition could be a more sensitive indicator of intervention than diversity alone.

Previous study has reported that oral administration of *Enterococcus faecium* can alleviate dextran sulfate sodium-induced colonic mucosal injury in mice by enhancing the expression of tight junction proteins, reducing inflammatory cell infiltration, and lowering the levels of TNF-α, IL-1β, and IL-6 in serum, thereby exerting anti-inflammatory effects [29]. In addition, supplementation with *Enterococcus faecium NCIMB 11181* has been shown to promote antibody production, restore intestinal villus architecture, and ameliorate dysbiosis [30]. These findings suggest that BXXXD may suppress esophageal mucosal inflammation and reverse precancerous lesions through microbiota-mediated mechanism.

4.3 Contribution of BXXXD components to the regulation of gut microbiota and SCFA metabolism

BXXXD is composed of seven herbs, and its chemical fingerprint analysis revealed the presence of various bioactive components. Several of these compounds have documented roles in microbiota and metabolic regulation. For instance, berberine has been confirmed by multiple studies to regulate the gut microbiota, enrich SCFA-producing bacteria, and improve intestinal barrier integrity [31]. Similarly, 6-shogaol has been reported to increase the abundance of butyrate-producing bacteria and upregulate butyrate metabolism in the gut [32]. Ginsenoside Rg1, another identified component, has been demonstrated to remodel gut microbiota diversity in mice fed with a high uric acid diet, increasing the levels of acetate, propionate, and butyrate while inhibiting the IL-17 and NF-κB signaling pathways, thereby alleviating intestinal inflammation [33]. These reported mechanisms align with changes observed in the present study following BXXXD intervention, including shifts in microbial composition, changes in SCFA, and activation of IL-17 signaling pathway. Together, these findings support the concept that the therapeutic effects of BXXXD may arise, at least in part, from the combined microbiota-modulating and immune-regulatory activities of its constituent compounds.

4.4 Gut microbiota composition, SCFA alterations, and microbial metabolic balance

Analysis of the gut microbiota further showed enrichment of *Escherichia-Shigella*, *Oscillibacter*, and *Ruminococcus* in the model group. *Escherichia-Shigella* is associated with metabolic syndrome and gut barrier disruption through endotoxin release and NF-κB activation [34], while *Oscillibacter and Ruminococcus* are known to produce harmful metabolites such as ammonia and phenol, which can compromise the integrity of intestinal epithelium [35]. These findings are consistent with the predicted enrichment of fatty acid synthesis and sulfur-containing amino acid metabolism in the model group, underscoring a shift toward a metabolically detrimental microbial profile.

In contrast, BXXXD-M group showed an increased relative abundance of genera typically associated with SCFA production or anti-inflammatory functions, including *Faecalibacterium*. Butyrate, for example, is known to block NF-κB signaling pathway, induce IL-10 secretion, and strengthen epithelial tight junctions [36]. However, enrichment of putative SCFA-producing taxa does not necessarily translate into higher circulating SCFA concentrations. In our study, despite the increased abundance of *Faecalibacterium*, serum butyrate levels did not increase, while serum acetate and total SCFA were elevated in model group and were reduced following BXXXD treatment. Since many beneficial effects of SCFA are mediated locally in the intestinal lumen and mucosa [37, 38], circulating SCFA level may reflect a balance among microbial production, epithelial uptake, host utilization, and barrier permeability, rather than microbial production alone. Indeed, excessively high systemic butyrate has been reported to attenuate the efficacy of anti-CTLA-4 treatment [39], suggesting that higher circulating SCFAs are not always indicative of improved host outcomes.

One possible explanation is that 4-NQO may compromise the integrity of intestinal-esophageal barrier, thereby facilitating the translocation of microbial metabolites into the systemic circulation. BXXXD treatment could help restore barrier function, thereby reducing excessive microbial fermentation and the resulting systemic accumulation of SCFA. Previous study has shown that butyrate synthesis primarily depends on the acetate CoA-transferase pathway, in which acetate serves as an essential substrate [40]. DUNCAN et al. [41] reported that approximately 85% – 90% of the carbon in butyrate produced by *Faecalibacterium prausnitzii* originated from exogenous acetate, implying that acetate was consumed to support local production of butyrate. Thus, we speculated that enrichment of *Faecalibacterium* after BXXXD treatment increased local acetate utilization in the intestinal lumen, while butyrate was preferentially consumed by colonocytes, resulting in reduced peripheral acetate without an overt increase in serum butyrate. Nevertheless, this interpretation remained indirect because luminal SCFA, epithelial uptake, and barrier function were not directly assessed in the present study. Future studies quantifying SCFA in both intestinal contents and serum, together with assessments of barrier integrity and metabolic flux, are warranted to validate these hypotheses.

Recent studies also suggest that acetate modulates metabolic adaptation under stress and influences neuroinflammation [42], raising the possibility that BXXXD may additionally exert effects through the gut-brain axis; however, this remains speculative and warrants further investigation as well.

4.5 Microbiota-initiated inflammation and its potential mechanisms in esophageal precancerous lesions

Transcriptome analysis of esophageal tissue showed enrichment of IL-17 signaling-related transcripts in both model and BXXXD-M groups. This overlap is not necessarily contradictory, because IL-17 signaling is context-dependent and can play dual roles in mucosal immunity. The relative abundance of opportunistic pathogens such as *Staphylococcus* and *Escherichia-Shigella* was positively correlated with IL-17A expression, suggesting that dysbiotic expansion of potential pathogens may contribute to IL-17-associated inflammatory responses. The gut microbiota and its metabolic products, including SCFA, have been shown to regulate the Th17/Treg balance and influence IL-17 signaling pathway [43]. The IL-17 signaling pathway is indispensable in mucosal immune defense, as its activation enhances antimicrobial immune responses and promotes epithelial repair [44]. It is also known to mediate mucosal inflammatory responses, enhance antimicrobial peptide production, and promote epithelial regeneration [45, 46]. Thus, IL-17 pathway enrichment in the model group may reflect pathogen-driven inflammation, whereas enrichment observed after BXXXD treatment may indicate a distinct, defense- and repair-associated IL-17 program rather than exacerbated inflammation. Notably, a moderate and well-regulated IL-17-mediated mucosal immune response may contribute to resistance against malignant transformation at the precancerous stage by enhancing epithelial barrier integrity, limiting persistent microbial stimulation, and reinforcing local immune surveillance. Although direct evidence linking these genera to esophageal precancerous lesions is still lacking, accumulating evidence from early-stage cancer and precancerous contexts suggests that alterations in the abundance of specific microbial taxa are associated with tumor-associated inflammatory phenotypes and changes in epithelial homeostasis [47–49]. A limitation of this study is that transcriptomic enrichment alone cannot distinguish

inflammatory versus repair-oriented IL-17 responses at the cellular level; future studies should validate key IL-17-axis molecules at the protein level and assess Th17/Treg dynamics and causality using targeted blockade or microbiota manipulation.

Based on the integrated findings from histopathology, microbiota profiling, metabolomics, and transcriptomic analyses, a schematic overview of the proposed mechanisms by which BXXXD alleviates esophageal precancerous lesions is summarized in Figure 9.

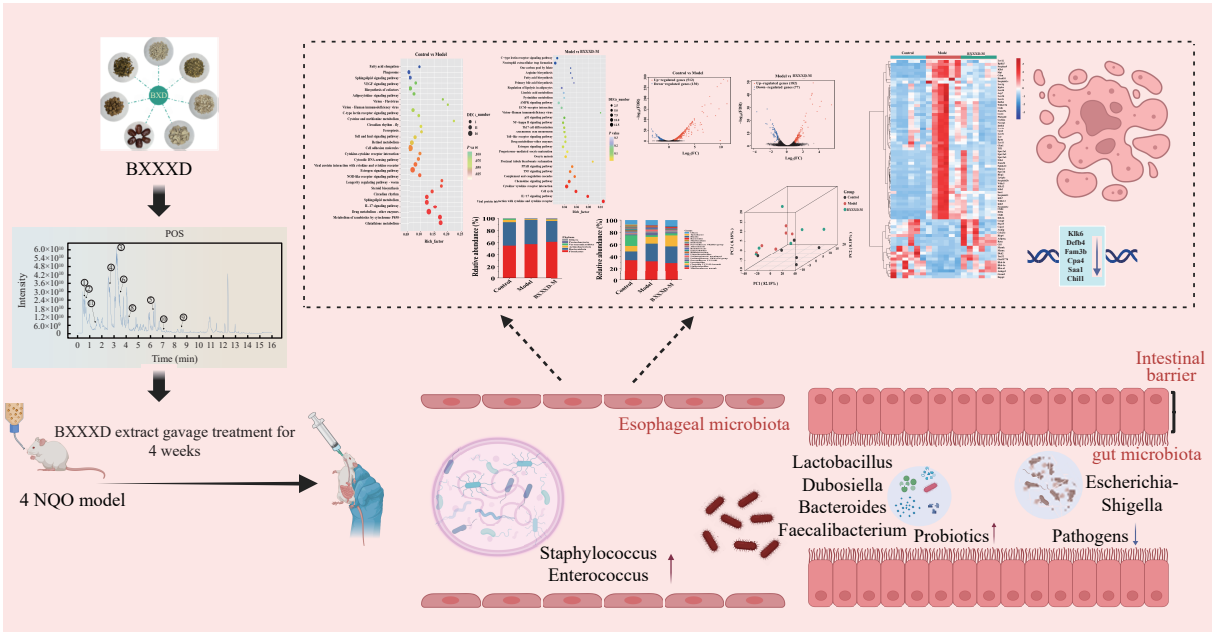

Figure 9 Alleviation of esophageal precancerous lesions by BXXXD through gut and esophageal microbiota regulation and homeostasis restoration

5 Conclusion

This study demonstrates that BXXXD effectively ameliorates 4-NQO-induced esophageal precancerous lesions in mice, with optimal efficacy observed at the medium dose (7.4 g/kg). Mechanistically, BXXXD treatment remodeled both esophageal and intestinal microbiota, enriching beneficial taxa such as *Enterococcus* and *Faecalibacterium* while reducing pathogenic bacteria including *Escherichia-Shigella*. These compositional shifts were accompanied by altered SCFA profiles and restoration of cross-ecosystem microbial interaction networks. Transcriptomic analysis revealed that BXXXD downregulated inflammation-related genes (*Klk6*, *Defb4*, *Fam3*b, *Cpa4*, *Saa1*, and *Chil1*) and modulated IL-17 signaling pathways. These findings indicate that BXXXD exerts therapeutic effects on esophageal precancerous lesions through microbiota modulation and immune regulation, providing mechanistic insights for its clinical application in esophageal cancer prevention.

Fundings

National Natural Science Foundation of China (82274369).

Ethical statement

All animal experiments were conducted in accordance with the Guidelines for the Care and Use of Laboratory Animals, and were approved by the Animal Ethics Committee of Nanjing University of Chinese Medicine (Ethics No. 202201A041).

Author contributions

Man Jin: software, formal analysis, validation, visualization, and writing – original draft. Wenfei Zhu: methodology, software, formal analysis, validation, and visualization. Zhaoling Wang: resources, data curation, investigation, and visualization. Kuai Yu: funding acquisition, software, formal analysis, and validation. Jianping Wu: investigation, data curation, formal analysis, and visualization. Junfeng Zhang: methodology, resources, funding acquisition, supervision, project administration, and writing – review & editing. All authors approved the submission and take responsibility for this manuscript.

Competing interests

Junfeng Zhang is an editorial board member for *Digital Chinese Medicine* and was not involved in the editorial

review or the decision to publish this article. All authors declare that there are no competing interests.

References

[1] SIEGEL RL, KRATZER TB, GIAQUINTO AN, et al. Cancer statistics, 2025. CA: A Cancer Journal for Clinicians, 2025, 75(1): 10–45.

[2] GAO J, WANG QM, FU FQ, et al. Comprehensive genomic and transcriptomic analyses reveal prognostic stratification for esophageal squamous cell carcinoma. Signal Transduction and Targeted Therapy, 2025, 10: 223.

[3] WHEELER JB, REED CE. Epidemiology of esophageal cancer. Surgical Clinics of North America, 2012, 92(5): 1077–1087.

[4] XIAO P, HUA ZL, KANG XY, et al. Influence of oral intaking habit on tongue coating microbiota in patients with esophageal precancerous lesions. Journal of Cancer, 2022, 13(4): 1168–1180.

[5] BABA YT, TAJIMA K, YOSHIMURA K. Intestinal and esophageal microbiota in esophageal cancer development and treatment. Gut Microbes, 2025, 17: 2505118.

[6] LI DR, LIU BQ, LI MH, et al. Dietary index for gut microbiota and risk of gastrointestinal cancer: a prospective gene-diet study. Nutrition Journal, 2025, 24(1): 81.

[7] CUI MY, YI X, CAO ZZ, et al. Targeting strategies for aberrant lipid metabolism reprogramming and the immune microenvironment in esophageal cancer: a review. Journal of Oncology, 2022, 2022: 4257359.

[8] LIU XY, LI B, LIANG LP, et al. From microbes to medicine: harnessing the power of the microbiome in esophageal cancer. Frontiers in Immunology, 2024, 15: 1450927.

[9] SU W, CHEN H, HU D, et al. The causal role of esophageal cancer and gut microbiota: a bidirectional Mendelian randomization study. Journal of Evidence-Based Integrative Medicine, 2025, 30: 2515690X251324793.

[10] ZOU Q, FENG LJ, CAI XC, et al. Esophageal microflora in esophageal diseases. Frontiers in Cellular and Infection Microbiology, 2023, 13: 1145791.

[11] ZHANG JW, ZHANG D, YIN HS, et al. *Fusobacterium nucleatum* promotes esophageal squamous cell carcinoma progression and chemoresistance by enhancing the secretion of chemotherapy-induced senescence-associated secretory phenotype via activation of DNA damage response pathway. Gut Microbes, 2023, 15: 2197836.

[12] KONG JY, LIU YW, QIAN MF, et al. The relationship between *Porphyromonas gingivalis* and oesophageal squamous cell carcinoma: a literature review. Epidemiology and Infection, 2023, 151: e69.

[13] SONG XB, GREINER-TOLLERSRUD OK, ZHOU HM. Oral microbiota variation: a risk factor for development and poor prognosis of esophageal cancer. Digestive Diseases and Sciences, 2022, 67(8): 3543–3556.

[14] MOREIRA C, FIGUEIREDO C, FERREIRA RM. The role of the microbiota in esophageal cancer. Cancers, 2023, 15(9): 2576.

[15] LUO YT, FU S, LIU YL, et al. Banxia Xiexin Decoction modulates gut microbiota and gut microbiota metabolism to alleviate DSS-induced ulcerative colitis. Journal of Ethnopharmacology, 2024, 326: 117990.

[16] JIANG YF, HUANG YQ, HU YN, et al. Banxia Xiexin Decoction delays colitis-to-cancer transition by inhibiting E-cadherin/β-catenin pathway via *Fusobacterium nucleatum* FadA. Journal of Ethnopharmacology, 2024, 328: 117932.

[17] TANG SM, LI N, WANG MX, et al. A clinical study on the treatment of advanced esophageal squamous cell carcinoma with modified Banxia Xiexin Decoction combined with the TP regimen. Journal of Traditional Chinese Medicine and Oncology, 2023, 5(3): 31–36.

[18] DU MB. Discussion on drug dosage in treatise on febrile diseases. China Journal of Chinese Materia Medica, 2019, 44(22): 5012–5016

[19] MAO SF, ZHANG J. Analysis of the effects of different decoction methods on the active ingredients in Banxia Xiexin Decoction. Chinese Herbal Medicines, 2019, 50(15): 3654–3659.

[20] XU SY, BIAN. Clinical Pharmacology. Shanghai: Shanghai Science and Technology Publishing House, 1988.

[21] YAO JC, CUI QH, FAN WY, et al. Single-cell transcriptomic analysis in a mouse model deciphers cell transition states in the multistep development of esophageal cancer. Nature Communications, 2020, 11: 3715.

[22] JIANG W, QIN N, CHEN T, et al. Immunomodulatory function of the active ingredients in traditional Chinese prescriptions on early stage esophageal cancer with dysplasia. American Journal of Translational Research, 2021, 13(3): 1667–1675.

[23] XIAO L, CHENG YQ, MA WS, et al. Huangqi Jianzhong Decoction improves gastric intestinal *Metaplasia* in rats by regulating the gut-thyroid axis. Phytomedicine, 2024, 135: 156174.

[24] XU ZJ, XIAO L, WANG SS, et al. Alteration of gastric microbiota and transcriptome in a rat with gastric intestinal *Metaplasia* induced by deoxycholic acid. Frontiers in Microbiology, 2023, 14: 1160821.

[25] SCHMIDT TS, HAYWARD MR, COELHO LP, et al. Extensive transmission of microbes along the gastrointestinal tract. eLife, 2019, 8: e42693.

[26] SINGH G, CHAUDHRY Z, BOYADZHYAN A, et al. Dysbiosis and colorectal cancer: conducive factors, biological and molecular role, and therapeutic prospectives. Exploration of Targeted Anti-Tumor Therapy, 2025, 6: 1002329.

[27] SONG W, LIN XF, XIA GH, et al. Altered gut microbiota and short-chain fatty acid in acute ischaemic stroke with active cancer. Stroke and Vascular Neurology, 2025: svn–2025–004217.

[28] MUJAKIĆ I, PIWOSZ K, KOBLÍŽEK M. Phylum gemmatimonadota and its role in the environment. Microorganisms, 2022, 10(1): 151.

[29] HE W, NI WJ, ZHAO JN. *Enterococcus faecium* alleviates gut barrier injury in C57BL/6 mice with dextran sulfate sodium-induced ulcerative colitis. Gastroenterology Research and Practice, 2021, 2021: 2683465.

[30] SHAO YJ, ZHEN WR, GUO FS, et al. Pretreatment with probiotics *Enterococcus faecium* NCIMB 11181 attenuated

Salmonella typhimurium-induced gut injury through modulating intestinal microbiome and immune responses with barrier function in broiler chickens. Journal of Animal Science and Biotechnology, 2022, 13(1): 130.

[31] ZHANG LC, WU XY, YANG RB, et al. Effects of berberine on the gastrointestinal microbiota. Frontiers in Cellular and Infection Microbiology, 2021, 10: 588517.

[32] ZHU HK, YANG DD, DU P, et al. 6-Shogaol improves the cognitive and memory declines of natural aging mice by modulating butyrate-producing microbiota and intestinal barrier. Phytomedicine, 2025, 148: 157381.

[33] SUN Q, LI ZM, YU Y, et al. Mechanism of ginsenoside Rg1 in regulating the metabolic function of intestinal flora for the treatment of high-purine dietary hyperuricemia. Nutrients, 2025, 17(11): 1844.

[34] ZHANG QJ, ZHANG LX, CHEN C, et al. The gut microbiota-artery axis: a bridge between dietary lipids and atherosclerosis? Progress in Lipid Research, 2023, 89: 101209.

[35] AMARETTI A, GOZZOLI C, SIMONE M, et al. Profiling of protein degraders in cultures of human gut microbiota. Frontiers in Microbiology, 2019, 10: 2614.

[36] LOUIS P, HOLD GL, FLINT HJ. The gut microbiota, bacterial metabolites and colorectal cancer. Nature Reviews Microbiology, 2014, 12(10): 661–672.

[37] HE YG, PENG K, TAN JZ, et al. Short-chain fatty acids and colorectal cancer: a systematic review and integrative Bayesian meta-analysis of microbiome-metabolome interactions and intervention efficacy. Nutrients, 2025, 17(22): 3552.

[38] ZHANG D, JIAN YP, ZHANG YN, et al. Short-chain fatty acids in diseases. Cell Communication and Signaling, 2023, 21(1): 212.

[39] COUTZAC C, JOUNIAUX JM, PACI A, et al. Systemic short chain fatty acids limit antitumor effect of CTLA-4 blockade in hosts with cancer. Nature Communications, 2020, 11: 2168.

[40] MARTÍN R, RIOS-COVIAN D, HUILLET E, et al. *Faecalibacterium*: a bacterial genus with promising human health applications. FEMS Microbiology Reviews, 2023, 47(4): fuad039.

[41] DUNCAN SH, HOLTROP G, LOBLEY GE, et al. Contribution of acetate to butyrate formation by human faecal bacteria. British Journal of Nutrition, 2004, 91(6): 915–923.

[42] HE QQ, JI LW, WANG YY, et al. Acetate enables metabolic fitness and cognitive performance during sleep disruption. Cell Metabolism, 2024, 36(9): 1998–2014. e15.

[43] CHENG HY, GUAN X, CHEN DK, et al. The Th17/treg cell balance: a gut microbiota-modulated story. Microorganisms, 2019, 7(12): 583.

[44] KUMAR P, MONIN L, CASTILLO P, et al. Intestinal interleukin-17 receptor signaling mediates reciprocal control of the gut microbiota and autoimmune inflammation. Immunity, 2016, 44(3): 659–671.

[45] MILLS KHG. IL-17 and IL-17-producing cells in protection versus pathology. Nature Reviews Immunology, 2023, 23(1): 38–54.

[46] LIANG SC, TAN XY, LUXENBERG DP, et al. Interleukin (IL)-22 and IL-17 are coexpressed by Th17 cells and cooperatively enhance expression of antimicrobial peptides. The Journal of Experimental Medicine, 2006, 203(10): 2271–2279.

[47] DIKEOCHA IJ, AL-KABSI AM, CHIU HT, et al. *Faecalibacterium prausnitzii* ameliorates colorectal tumorigenesis and suppresses proliferation of HCT116 colorectal cancer cells. Biomedicines, 2022, 10(5): 1128.

[48] ESFANDIARI F, BAKHSHI B, SHAHBAZI T, et al. Significant difference in gut microbiota *Bifidobacterium* species but not *Lactobacillus* species in colorectal cancer patients in comparison with healthy volunteers using quantitative real-time PCR. PLoS One, 2024, 19(11): e0294053.

[49] ELAHI Z, SHARIATI A, BOSTANGHADIRI N, et al. Association of *Lactobacillus*, *Firmicutes*, *Bifidobacterium, Clostridium*, and *Enterococcus* with colorectal cancer in Iranian patients. Heliyon, 2023, 9(12): e22602.

(Editor-in-Charge Siyi Wei)

半夏泻心汤通过调节肠道菌群缓解小鼠食管癌前病变的机制研究

靳曼[a†], 朱雯菲[a†], 王召玲[a], 虞快[a], 吴剑平[a, b], 张军峰[a*]

a. 南京中医药大学医学院, 江苏 南京 210023, 中国
b. 南京中医药大学实验动物中心, 江苏 南京 210023, 中国

【摘要】目的 探讨半夏泻心汤（BXXXD）治疗食管癌前病变的微生物学机制。**方法** 将 30 只无特定病原体（SPF）级雌性 C57BL/6J 小鼠分为对照组（ 6 只）和 4-硝基喹啉 1-氧化物（4-NQO）暴露组（24 只）。4-NQO 暴露组小鼠给予含 4-NQO（100 μg/mL）的饮水，连续 17 周，以诱导食管癌前病变，而对照组则饮用无菌饮用水。在模型建立后，4-NQO 暴露组小鼠被进一步分为模型组和 3 个 BXXXD 处理组，包括低剂量（BXXXD-L，3.7 g/kg）、中剂量（BXXXD-M，7.4 g/kg）、高剂量（BXXXD-H，14.8 g/kg）组（每组 6 只）。在接下来的干预期内，对照组和模型组的小鼠每天通过灌胃给予无菌水，而 BXXXD 组的小鼠则每天分别灌胃对应剂量的 BXXXD 水提取物，持续 4 周。通过苏木精-伊红（HE）染色观察食管组织的组织学变化；通过 16S rDNA 高通量测序分析小鼠粪便和食管微生物群落，评估细菌多样性、群落结构和共现网络。使用超高效液相色谱-四极杆静电场轨道阱高分辨质谱（UHPLC-QE-MS）分析 BXXXD 的化学指纹；通过气相色谱-质谱联用（GC-MS）定量分析血清短链脂肪酸（SCFA）水平。对食管组织进行转录组分析，以评估基因表达谱。**结果** 与模型组相比，BXXXD-M 组小鼠食管黏膜层增殖减轻，细胞排列更为整齐，治疗效果优于 BXXXD-L 组和 BXXXD-H 组。菌群分析显示，在食管中，BXXXD 干预升高食管有益菌肠球菌属丰度，降低病原性 *Escherichia-Shigella* 丰度；在肠道中，升高肠道乳酸杆菌属（*Lactobacillus*）、杜氏杆菌属（*Dubosiella*）、拟杆菌属（*Bacteroides*）、粪杆菌属（*Faecalibacterium*）等有益菌相对丰度。靶向代谢组学分析显示，BXXXD 干预显著降低 SCFA 水平。食管基因表达谱显示，BXXXD 可降低激肽释放酶相关肽酶 6（*Klk6*）、防御素 β4（*Defb4*）、序列相似家族 3 成员 B（*Fam3b*）、羧肽酶 A4（*Cpa4*）、血清淀粉样蛋白 A1（*Saa1*）、几丁质酶-3 样蛋白 1（*Chil1*）等与食管癌进展、迁移和侵袭相关基因的表达水平。**结论** 半夏泻心汤可能通过调节肠道菌群及其代谢物降低食管癌相关基因表达水平，从而改善食管癌前病变。

【关键词】半夏泻心汤；食管癌前病变；肠道菌群；转录组；短链脂肪酸